Map segmentation, automated model-building and their application to the Cryo-EM Model Challenge

Thomas C. Terwilliger[1,2], Paul D. Adams[3,4], Pavel V. Afonine[3,5], Oleg V. Sobolev[3]

[1]*Los Alamos National Laboratory, Los Alamos NM 87545 USA*
[2]*New Mexico Consortium, Los Alamos NM 87544 USA*
[3]*Molecular Biophysics & Integrated Bioimaging Division, Lawrence Berkeley National Laboratory, Berkeley, CA 94720-8235, USA*
[4]*Department of Bioengineering, University of California Berkeley, Berkeley, CA, USA*
[5]*Department of Physics and International Centre for Quantum and Molecular Structures, Shanghai University, Shanghai, 200444, People's Republic of China*

E-mail: tterwilliger@newmexicoconsortium.org

Abstract

A recently-developed method for identifying a compact, contiguous region representing the unique part of a density map was applied to 218 cryo-EM maps with resolutions of 4.5 Å or better. The key elements of the segmentation procedure are (1) identification of all regions of density above a threshold and (2) choice of a unique set of these regions, taking symmetry into consideration, that maximize connectivity and compactness. This segmentation approach was then combined with tools for automated map sharpening and model-building to generate models for the 12 maps in the 2016 cryo-EM model challenge in a fully automated manner. The resulting models have completeness from 24% to 82% and rms differences from reference interpretations of 0.6 Å to 2.1 Å.

Introduction

In the 2016 Cryo-EM Modeling Challenge (see http://challenges.emdatabank.org/?q=model_challenge; accessed 2017-11-19), a total of 12 maps were supplied to contestants along with reconstruction symmetry and the sequences of the molecules present. One of the goals of the Challenge was to fully interpret such a map given only the map, the symmetry and the sequence information. There are a number of tools being developed by several groups for automated interpretation of cryo-EM maps (DiMaio and Chiu, 2016). These include methods for identification of secondary structure (Jiang et al., 2001; Kong and Ma, 2003; Kong et al., 2004; Baker, Ju and Chiu, 2007), methods for combination of structure-modeling tools such as Rosetta with cryo-EM model-building (Lindert et al., 2012; Wang et al., 2015; Frenz et al., 2017), semi-automated tools for full map interpretation (Baker et al., 2011), and automated tools based on chain-tracing (Chen et al., 2016; Collins and Si, 2017) and template-matching approaches (Zhou, Wang and Wang, 2017).

Prior to the 2016 cryo-EM Model Challenge, we had begun development of software for automatic map sharpening (*phenix.auto_sharpen;* Terwilliger et al., 2018a) and interpretation of density in cryo-EM maps (*phenix.map_to_model;* Terwilliger et al., 2018b*)* as part of the *Phenix* software package (Adams et al, 2010). It was possible in principle to apply these tools directly to the 2016 Challenge, interpreting an entire map and ignoring the symmetry of the map. It seemed however that it would be more efficient to identify a unique part of map that contained a complete molecule, to interpret that part of the map, and then to expand the result using the symmetry in the map to represent the entire map. Powerful tools existed for map segmentation (e.g., Volkmann, 2002; Baker, Chiu and Bajaj, 2006; Yu and Bajaj, 2008; Pintilie et al., 2010), but we wanted to be able to integrate the segmentation and symmetry analysis with automated model-building so that information from model-building could be used to make the final choice of the regions of density representing a single molecular unit. We therefore developed a new *Phenix* tool, *segment_and_split_map* (Terwilliger et al., 2018b) which could be used for this purpose. Here we describe the application of *segment_and_split_map* to a set of 218 cryo-EM maps selected to generally represent the unique currently-available cryo-EM maps with resolution of 4.5 Å or better. We then describe map segmentation, sharpening, and model-building (Terwilliger et al., 2018b) applied to the 12 cryo-EM maps in the 2016 Cryo-EM Model Challenge.

Methods

Summary of map segmentation

The main goal of our segmentation procedure is to identify the density in a map that corresponds to the unique part of that map. A secondary goal is to choose this density in such a way that it corresponds as closely as possible to the unique biological unit in the map. Our overall approach to map segmentation is (1) to identify all regions of density above an automatically-determined threshold, and (2) to choose a unique set of density regions that maximizes connectivity and compactness, taking into account the symmetry that is present. By default, the process repeated with a new threshold after removing the density that has been used in the first iteration.The details of this segmentation procedure have recently been described (Terwilliger et al., 2018b).

Symmetry present in a map

We identified symmetry relationships that were applied during map reconstruction to a using a simplified version of approaches described by Zhang et al., (2012). In many cases the symmetry applied during reconstruction is specified in the EM Data Bank (EMDB; Lawson et al., 2016; as for example “I” for icosahedral reconstructions, “C6” for a 6-fold symmetry axis). In others, the symmetry is specified in meta-data associated with the deposited model in the Protein Data Bank (PDB; Bernstein et al., 1977; Berman et al., 2000). In still others, the model deposited in the PDB contains symmetry-related copies which we extracted with the *Phenix* tool

phenix.simple_ncs_from_pdb. If present, we used symmetry from the deposited models and their meta-data, and if not, we used the information from the EMDB or literature specified in the deposition and the assumption that principal symmetry axes (i.e., screw axes, rotational axes) are generally along the principal axes of the reconstruction to find reconstruction symmetry in the density maps.

Map-model correlations

We calculated map-model correlations using the *Phenix* tool *map_model_cc*. This tool identifies the region occupied by the model as all grid points in the target map within a specified distance (typically 3 Å) of an atom in the model. Then it generates a model-based map on the same grid based on the model and calculates the correlation of density values between the target map and the model-based map inside the region occupied by the model.

Data used for map segmentation

We selected a group of 218 cryo-EM maps to test our segmentation algorithms. We started with 492 maps we could extract from the EMDB in August of 2017 with simple *Phenix* tools and that were reconstructed at resolutions of 4.5 Å or better. We excluded 91 maps where the resolution in the EMDB and PDB differed by 0.2 Å or more or was not reported, 24 maps where the map-model correlation was less than 0.3, and 16 maps for which the signal-to-noise in map sharpening (Terwilliger et al., 2018a) was less than 3. We then removed map-model pairs that were largely duplications by clustering based on sequence identity using a cutoff of 95% identity and choosing the highest-resolution representative of each group. Four of the maps in this set were associated with two models, so one map-model pair was set aside for each of these, yielding 218 map-model pairs that were analyzed in this work.

Evaluating the results of map segmentation by calculation of fraction of molecular unit within the segmented region

We estimated the fraction of the molecular unit within the segmented region of a map from a comparison of map-model correlations. Our method is related to the cross-correlation variation metric described by Zhang et al. (2012) but it is extended to make an estimate of the fraction of the molecular unit that matches the segmented map. The segmented map has values of zero everywhere outside the segmented region of the map. The overall idea is that if the segmented region contains a complete molecular unit, then the map-model correlation between one complete molecular unit and the segmented map will be the same as the map-model correlation with the original map. On the other hand, if the segmented region contains part of one molecular unit and parts of symmetry-related ones, then the map-model correlation between one intact molecular unit and the segmented map will be lower than the correlation to the original map. We use this difference in map correlation to estimate the fraction of a complete molecule that is within the segmented region.

We first calculated the map-model correlation between the original map and a map calculated from single molecular unit extracted from the deposited model of the structure. Then we calculated the map-model correlation between the segmented map and a single molecular unit. The square of the ratio of these correlations is (see below) approximately equal to the fraction of the molecular volume that is within the segmented map. The single molecular unit to compare with the map was chosen to be a set of chains representing the unique part of the deposited model. In cases with symmetry, each symmetry-related choice of molecular unit was considered and the one with the highest map-model correlation was chosen.

The relationship between the map-model correlation for a single molecular unit and the original map compared to the correlation for a molecular unit and a segmented map can be calculated in a straightforward fashion with one assumption. This assumption is that the local map-model correlation for the original map and this single molecular unit is approximately the same everywhere in the region of the model. With this assumption, we can readily calculate the effect of setting all but a fraction *f* of the map density in the region of the model to zero. This corresponds to calculating the map-model correlation of the segmented map to one full molecular unit, where a fraction *f* of the molecular unit is present in the segmented map.

The correlation coefficient CC between two maps with density values represented by D_1 and D_2 can be written (after adjusting each map to set the mean density for each to zero so that $< D_1> = < D_2> =0$) as,

$$CC = < D_1D_2>/\mathrm{sqrt}(<D_1^2> <D_2^2>) \quad , \qquad (1)$$

where the calculation in this case is carried out over all the grid points near the model. Now suppose we create a new map D_1' in which we set D_1 to zero at a fraction (1-*f*) of these grid points. Referencing Eq. (1), this means that the values of $D_1'D_2$ and $D_1'^2$ will be zero at all these grid points, but D_2^2 will be the same. Assuming then that the values of $< D_1D_2>$, $<D_1^2>$, and $<D_2^2>$ are approximately the same everywhere near the model, we can write that the map-model correlation for the segmented map (CC') with all but (1-*f*) of the map set to zero is related to the map-model correlation for the original map (CC) by,

$$CC' = CC\ \mathrm{sqrt}(f) \ , \qquad (2)$$

so that *f*, the fraction inside the mask, is approximately given by $f = CC'^2/CC^2$.

Data used from the Cryo-EM Model Challenge

The maps and reconstruction symmetry used for the 12 cryo-EM maps in the 2016 Cryo-EM Model Challenge were taken from the Model Challenge site at http://challenges.emdatabank.org/?q=model_challenge (accessed 2017-11-19). The Challenge consisted of 8 unique molecules, four of which were associated with two maps at different

resolutions, leading to 12 different maps (Table I). Of these maps, most were associated with previously-deposited models that were likely to be more accurate than the ones we built automatically and that were therefore suitable for use as references for the accuracy of our models. For one additional map (groEL, EMDB entry 6422) there was no deposited model, however there is a model for a related structure in the PDB (1ss8) which we offset superimposed on this map and used as a reference. One final structure was recently interpreted (the proteasome structure; Veesler, D., unpublished) and we used that structure as a reference model. We checked the map-model agreement with *phenix.map_model_cc* and these map-model correlations ranged from 0.34 (rather low, supporting only low confidence in the model), to 0.85, suggesting that the model is in good agreement with the map.

Results and Discussion

Fig. 1 illustrates the application of our map segmentation procedure (Terwilliger et al., 2018b) to the 2.9 Å cryo-EM reconstruction of the anthrax protective antigen pore (Jiang et al., 2015). The map has C7 symmetry (a 7-fold symmetry axis). Fig. 1A shows the 7-fold symmetry of the pore and illustrates one of the 7 chains in purple. Fig. 1B shows the density map with 7-fold symmetry. It can be seen that the density is much stronger for the extracellular of the molecule than for the transmembrane part below. The 7-fold symmetry was used along with the map to identify symmetry-related regions of density in the map. Then a compact and connected unique set of density regions was chosen to represent the molecule. Fig. 1C shows the individual segmented regions of the map, and Fig. 1D shows the segmented region, augmented by neighboring regions of density.

We then applied our segmentation procedure to a large set of cryo-EM maps from the EMDB (Fig. 2). As expected, using the reconstruction symmetry of the maps in segmentation often resulted in a very large reduction in the volume that needed to be considered to include the unique part of each map (Fig. 2A). The average volume after segmentation and placing the unique segmented region in a new box was 8% of the starting volume of the maps. In most (206 of 218) of the cases illustrated in Fig. 2 we used the *add_neighbors* procedure to add a layer of regions around the unique molecular volume in order to increase the chance of finding a complete molecule. The 12 cases where this was not done were those where the map was very large and we attempted to keep the size of the region to be worked on to the minimum possible.

Fig. 2B illustrates the fraction of the unique molecular unit that is within the unique segmented region used for each map in Fig. 2A. This fraction of the molecule contained within the segmented region is estimated from the map-model correlation between the molecule and a map which is set to zero everywhere outside the segmented region, normalized to the map-model correlation without setting any of the map to zero. If the molecule is within the segmented region this normalized correlation will be unity, while if the molecule is split between different segmented regions it will be smaller. As shown in Fig 2B, the fraction within a single segmented region varies considerably among the 218 maps analyzed here, but the

mean fraction was 0.72, indicating that typically a large fraction, but not all, of the molecular unit was contained within the segmented region.

We applied the combination of map sharpening, segmentation, and model-building as implemented in the *Phenix* tool *map_to_model* (Terwilliger et al., 2018b) to the 12 maps in the 2016 cryo-EM Challenge. The maps and corresponding reference models are listed in Table I along with the CPU hours required for the analysis, which ranged from 7 to 422 hours. Table II lists the number of residues that were built with C_α or P atoms within 3 Å of the corresponding atoms in the reference model by the *map_to_model* procedure, along with the fraction of the reference model represented by the model that was built and the fraction of residues that were assigned the correct residue identity. The number of residues built more than 3 Å from any residue in the reference model is also listed.

Overall, from 35% to 82% of the protein portions of the 12 structures were built within 3 Å of the corresponding reference models. For the two RNA structures, 24% and 54% of the RNA portions were built within 3 Å of the corresponding reference models. From 5% to 75% of the protein and RNA sequences were correctly assigned. For the non-ribosome structures, only a small proportion of the models built did not correspond at all to the deposited models. On the other hand, for the ribosome structures, a large fraction (over half for the 3.6 Å map) of the protein residues built did not correspond to the deposited models. Most of these incorrectly-built residues are located in regions that are RNA in the deposited models (recently we have developed a tool, *phenix.remove_poor_fragments* that can remove some of these incorrectly-built residues, but it was not available at the time of this work, TT, OS, PDA and PVA, unpublished). The models built by *phenix.map_to_model* have rms differences from reference interpretations of 0.6 Å to 2.1 Å.

The procedures developed here for map segmentation could be applied automatically to all of the 218 maps that we examined in the tests shown in Fig. 2. Further, all 12 of the maps in the 2016 Cryo-EM Model Challenge could be automatically sharpened, segmented and partially interpreted by the *phenix.map_to_model* procedure. It seems likely that combining the techniques developed here with other approaches for automatic model-building might lead to procedures that can automatically interpret an even larger part of cryo-EM maps.

Acknowledgements

This work was supported by the NIH (grant GM063210 to PDA and TT) and the Phenix Industrial Consortium. This work was supported in part by the US Department of Energy under Contract No. DE-AC02-05CH11231 at Lawrence Berkeley National Laboratory. This research used resources provided by the Los Alamos National Laboratory Institutional Computing Program, which is supported by the U.S. Department of Energy National Nuclear Security Administration under Contract No. DE-AC52-06NA25396.Molecular graphics and analyses were performed with the UCSF *Chimera* package (Petterson et al., 2005) and with *Coot* (Emsley et al., 2010). Chimera

is developed by the Resource for Biocomputing, Visualization, and Informatics at the University of California, San Francisco (supported by NIGMS P41-GM103311).

Figure Legends

Figure 1. Segmentation of density for the anthrax protective antigen pore. A. Deposited structure of anthrax protective antigen pore one of the 7 chains in purple. B. Density map illustrating the 7-fold symmetry used in the reconstruction. C. Individual segmented regions of the map superimposed on a single chain from the deposited structure. Note that the deposited structure was not used in the segmentation process. D. Illustration of the segmented region, augmented by neighboring regions of density.

Figure 2. Application of segmentation procedure to cryo-EM maps from the EMDB. A. Fraction of original map required to represent the segmented region of each map. B. Fraction of each molecular unit contained within the segmented region of each map.

References

Adams, P. D., Afonine, P.V., Bunkóczi, G., Chen, V.B., Davis, I.W., Echols, N., Headd, J.J., Hung, L.-W. Kapral, G.J., Grosse-Kunstleve, R.W., McCoy, A.J., Moriarty, N.W., Oeffner, R., Read, R.J., Richardson, D.C., Richardson, J.S., Terwilliger, T.C. & Zwart, P.H., 2010. PHENIX: a comprehensive Python-based system for macromolecular structure solution. Acta Cryst., D66, 213-221.

Baker, M.L., Yu, Z., Chiu, W., Bajaj, C., 2006. Automated segmentation of molecular subunits in electron cryomicroscopy density maps. J. Structural Biology 156, 432-441.

Baker, M.L., Ju, T., Chiu, W., 2007. Identification of secondary structure elements in intermediate-resolution density maps. Structure 15, 7–19.

Baker, M.L., Abeysinghe, S.S., Schuh, S., Coleman, R.A., Abrams, A., March, M.P., Hyrc, C.F., Ruths, T., Chiu, W., Ju, T. (2011). Modeling protein structure at near atomic resolutions with Gorgon. J. Struct. Biol. 174, 360-373.

Berman, H.M., Westbrook, J., Feng, Z., Gilliland, G., Bhat, T.N., Weissig, H., Shindyalov, I.N. and Bourne, P.E., 2000. The Protein Data Bank. Nucleic Acids Research, 28, 235-242.

Bernstein, F.C., Koetzle, T.F., Williams, G.J., Meyer, E.F., Jr., Brice, M.D., Rodgers, J.R., Kennard, O., Shimanouchi, T. and Tasumi, M., 1977. The Protein Data Bank: a computer-based archival file for macromolecular structures. J. Mol. Biol. 112, 535-542.

Collins, P., Si, D. (2017). A graph based method for the prediction of backbone trace from cryo-EM density maps. ACM-BCB '17 Proceedings of the 8th ACM International Conference on Bioinformatics, Computational Biology,and Health Informatics.

Chen, M., Baldwin, P.R., Ludtke, S.J., Baker, M.L., 2016. De Novo modeling in cryo-EM density maps with Pathwalking. J. Structural Biol. 196, 289-298.

DiMaio, F., Chiu, W. (2016). Tools for model building and optimization into near-atomic resolution electron cryo-microscopy density maps. Methods. Enzymol. 679, 255-276.

Emsley, P., Lohkamp, B., Scott, W. G. & Cowtan, K. (2010). Features and development of Coot. Acta Cryst. D66, 486-501.

Frenz, B., Walls, A.C., Egelman, E.H., Veesler, D., DiMaio, F., 2017. RosettaES: a sampling strategy enabling automated interpretation of difficult cryo-EM maps. Naure Methods 14, 797-803.

Jiang, W., Baker, M.L., Ludtke, S.J., Chiu, W., 2001. Bridging the information gap: computational tools for intermediate resolution structure interpretation. J. Mol. Biol. 308, 1033–1044.

Atomic structure of anthrax protective antigen pore elucidates toxin translocation
Jiang J., Pentelute B.L., Collier R.J., Zhou, Z.H., 2015. Atomic structure of anthrax protective antigen pore elucidates toxin translocation. Nature 521, 545-549.

Kong, Y., Ma, J., 2003. A structural-informatics approach for mining beta-sheets: locating sheets in intermediate-resolution density maps. J. Mol. Biol. 332, 399–413.

Kong, Y., Zhang, X., Baker, T.S., Ma, J., 2004. A Structural-informatics approach for tracing beta-sheets: building pseudo-C(alpha) traces for beta-strands in intermediate-resolution density maps. J. Mol. Biol. 339, 117–130.

Lawson C.L., Baker, M.L, Best, C., Bi, C., Dougherty, M., Feng, P., van Ginkel, G., Devkota, B, Lagerstedt, I., Ludtke, S.J., Newman, R.H., Oldfield, T.J., Rees, I., Sahni, G., Sala, R., Velankar, S., Warren, J., Westbrook, J.D., Henrick, K., Kleywegt, G.J., Berman, H.M., Chiu, W. 2016. EMDataBank unified data resource for 3DEM. Nucleic Acids Res. 44, D396–D403.

Lindert, S., Alenxander, N., Wotzel, N., Karakas, M., Stewart, P.L., Meiler, J., 2012. Em-Fold: De novo atomic-detail protein structure determination from medium-resolution density maps. Structure 20, 464-478.

Pettersen E.F., Goddard T.D., Huang C.C., Couch G.S., Greenblatt D.M., Meng E.C., Ferrin, T.E. 2004. UCSF Chimera--a visualization system for exploratory research and analysis. J Comput. Chem. 25, 1605-1612.

Pintilie, G. D., Zhang, J., Goddard, T. D., Chiu, W., & Gossard, D. C., 2010. Quantitative analysis of cryo-EM density map segmentation by watershed and scale-space filtering, and fitting of structures by alignment to regions. Journal of Structural Biology 170, 427–438.

Terwilliger, T.C., Sobolev, O., Afonine, P.V., Adams, P.D. (2018a). Automated map sharpening by maximization of detail and connectivity. bioRxiv doi: https://doi.org/10.1101/247049.

Terwilliger, T.C., Adams, P.D., Afonine, P.V., Sobolev, O.V. (2018b). A fully automatic method yielding initial models from high-resolution electron cryo-microscopy maps. bioRxiv doi: https://doi.org/10.1101/267138

Volkmann, N. (2002). A novel three-dimensional variant of the watershed transform for segmentation of electron density maps. J. Struct. Biol. 138, 123–129.

Wang, R. Y-R., Kudryashev, M., Li, X., Egelman, E.H., Basler, M., Cheng, Y., Baker, D., DiMaio, F., 2015. De novo protein structure determination from near-atomic-resolution cryo-em maps. Nature Methods 12, 335-341.

Yu, Z., Bajaj, C. (2008). Computational approaches for automatic structural analysis of large biomolecular complexes. IEEE/AC Transactions on computational bology and bioinformatics 5 568-582.

Zhang, Q., Bettadapura, R., Bajaj, C. (2012). Macromolecular structure modeling from 3D EM using VolRover 2.0. Biopolymers 97, 709-731.

Zhou N., Wang, H., Wang, J., 2017. EMBuilder: A Template Matching- based automatic model-building program for high-resolution cryo-electron microscopy maps. Scientific Rep. 7, 2664.

Table I. Cryo-EM Challenge structures analyzed with *map_to_model*

Structure	Map (EMDB entry)	Reference model (PDB entry[1])	Resolution (Å)	Reference map-model correlation
Beta galactosidase	2984	5A1A	2.2	0.73
Proteasome	6287	undeposited	2.8	0.81
E. coli 70S ribosome	2847	5AFi	2.9	0.85
Beta galactosidase	5995	3J7H	3.2	0.76
Proteasome	5623	3J9i	3.3	0.77
trpV1	5778	3J5P	3.3	0.56
TMV	2842	4UDV	3.4	0.73
Gamma secretase	3061	5A63	3.4	0.41
E. coli 70S ribosome	6316	3JA1	3.6	0.38
Brome mosaic virus	6000	3J7L	3.8	0.76
GroEL	6422	1SS8	4.1	0.83
Gamma secretase	2677	5A63	4.5	0.34

[1] The PDB codes are written following the convention outlined in the editor's notes in the Computation Crystallography Newsletter (Comput. Cryst. Newsl. 2015:6; https://www.phenix-online.org/newsletter/CCN_2015_07.pdf).

Table II. Results of Cryo-EM Challenge analysis with *map_to_model*

Structure	Reso-lution (Å)		Built within 3 Å (Residues)	Rmsd (Å)	Built (%)	Matched to sequence (%)	Built further than 3 Å (Residues)
Beta galactosidase	2.2		842	0.6	82	75	10
Proteasome	2.8		327	0.6	78	59	3
E. coli 70S ribosome	2.9	Protein	3212	0.7	51	23	2112
		RNA	2566	1.0	54	49	280
Beta galactosidase	3.2		676	1.2	66	23	26
Proteasome	3.3		246	1.2	58	48	4
trpV1	3.3		330	0.8	56	30	18
TMV	3.4		76	1.3	50	34	8
Gamma secretase	3.4		832	1.0	68	24	80
E. coli 70S ribosome	3.6	Protein	2479	2.0	35	8	3979
		RNA	1140	1.9	24	26	440
Brome mosaic virus	3.8		198	1.5	41	11	14
GroEL	4.1		309	1.3	59	16	10
Gamma secretase	4.5		619	2.1	51	8	185

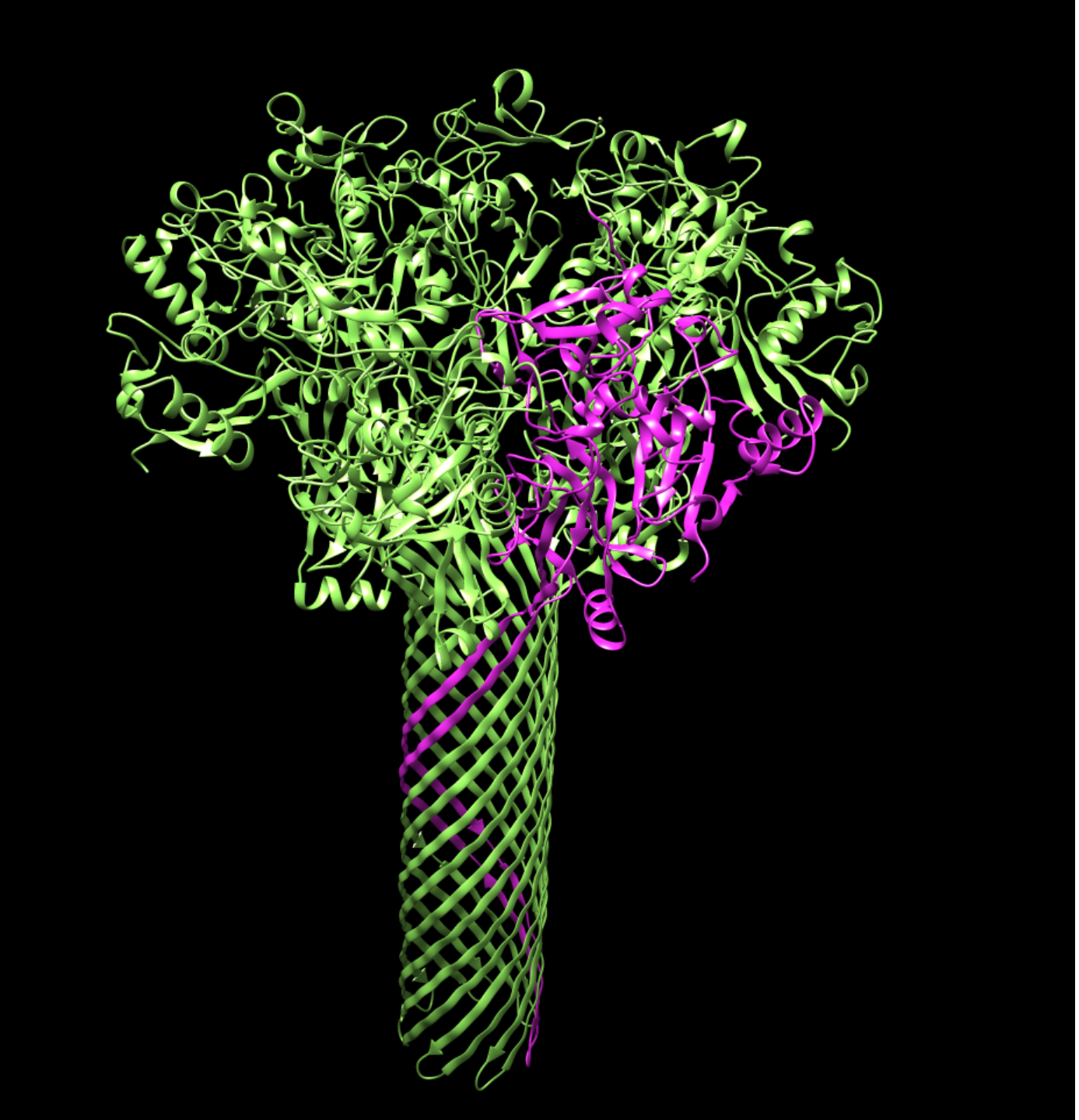

Fig 1A

Fig 1B

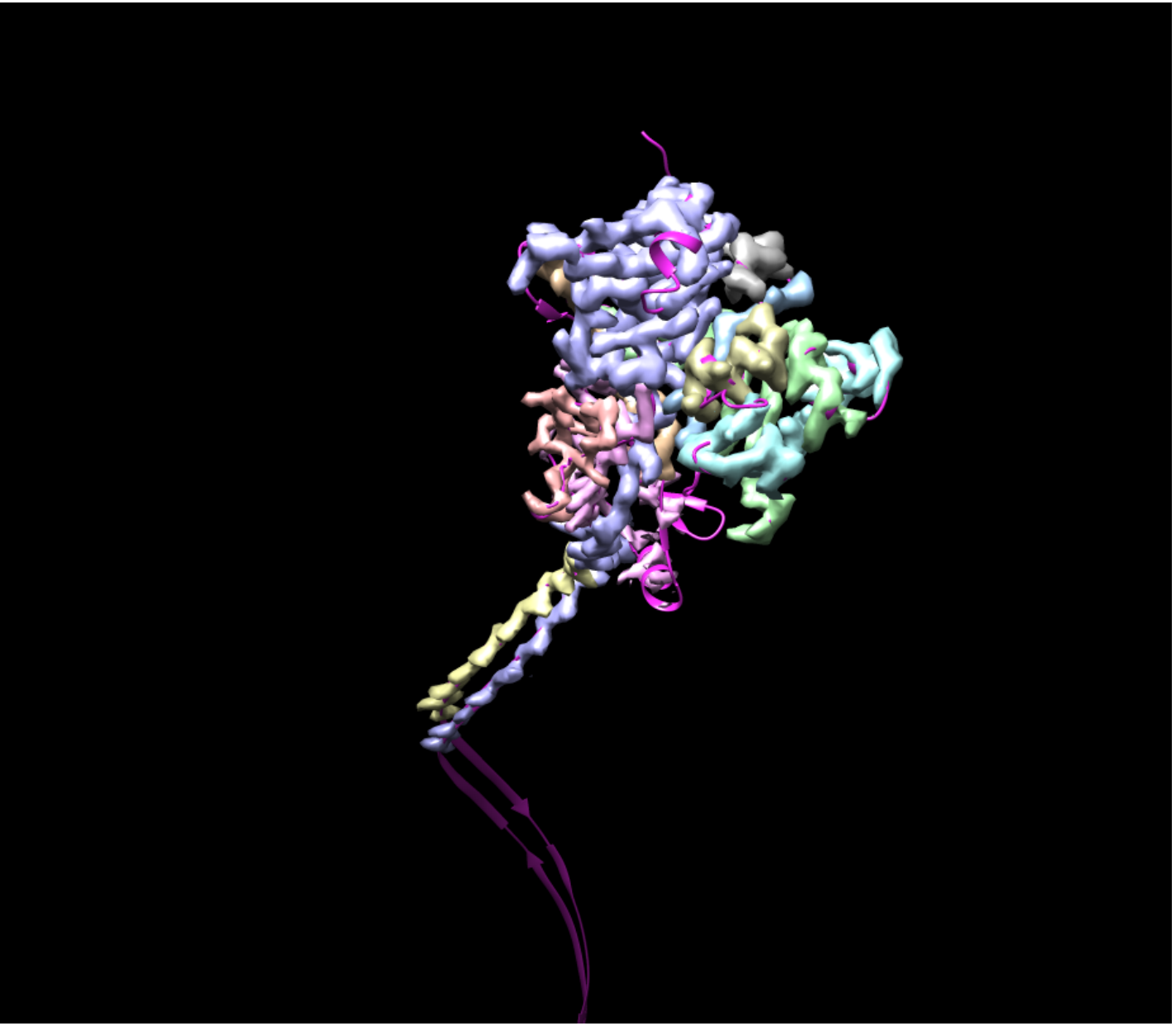

Fig 1C

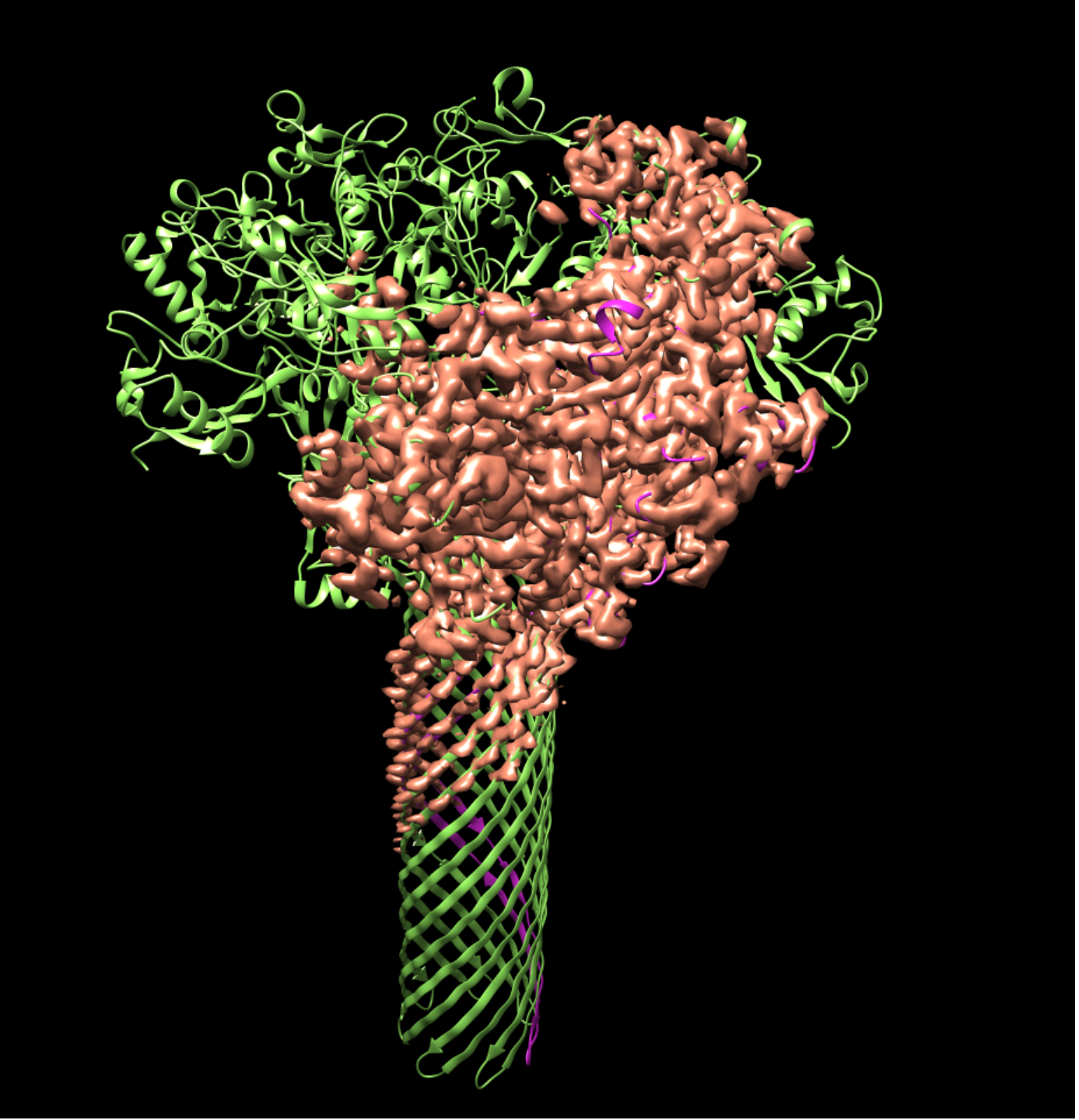

Fig 1D

Fig 2A

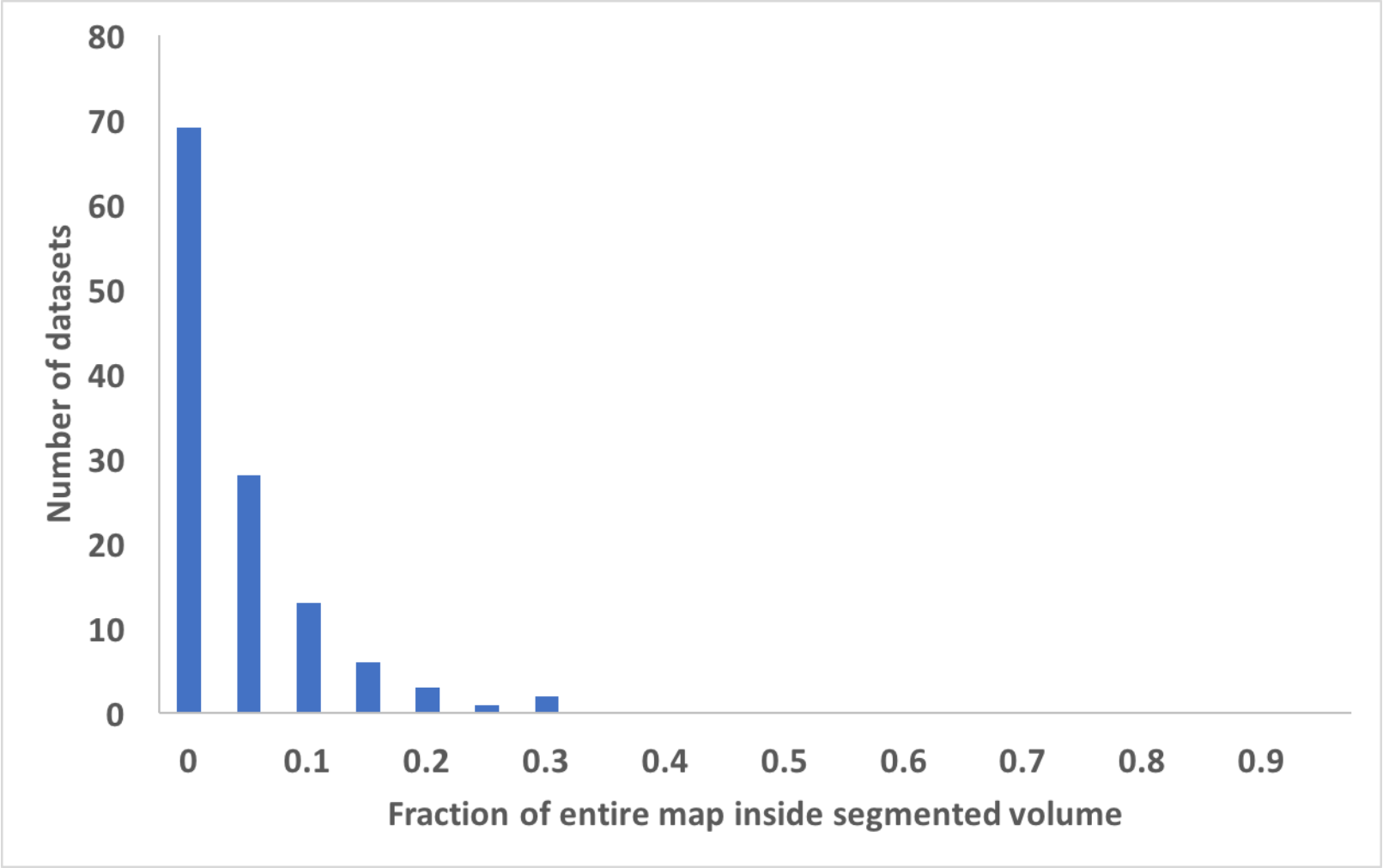
80
70
60
50
40
30
20
10
0
Number of datasets
0
0.1
0.2
0.3
0.4
0.5
0.6
0.7
0.8
0.9
Fraction of entire map inside segmented volume

Fig 2B

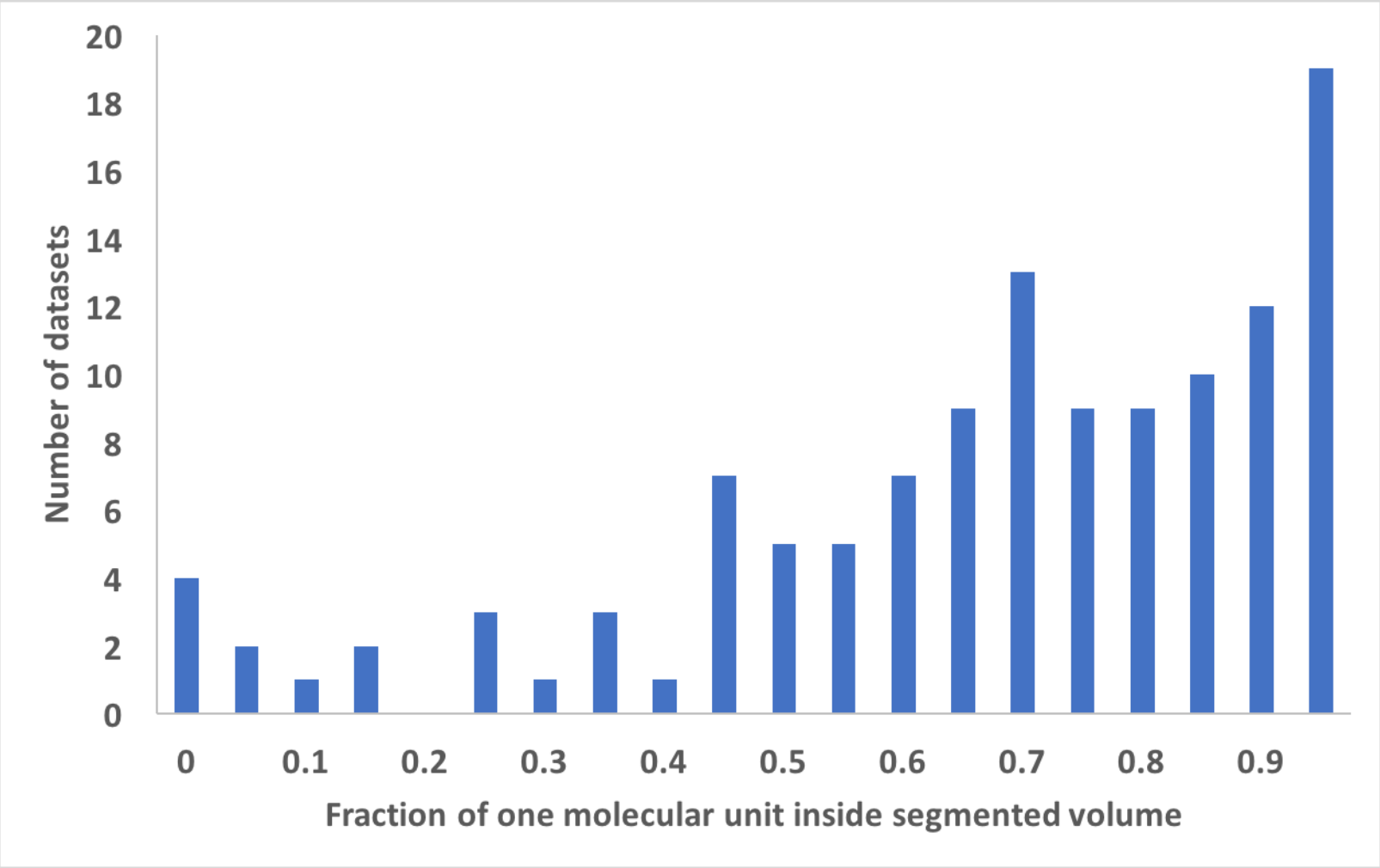
Number of datasets
20
18
16
14
12
10
8
6
4
2
0
0
0.1
0.2
0.3
0.4
0.5
0.6
0.7
0.8
0.9
Fraction of one molecular unit inside segmented volume